Supporting Information

Schulz et al. 10.1073/pnas.1206036109

SI Text

Materials and Methods. ***SproutCounter software.*** For the automatic evaluation of cell sprouting under various conditions, image analysis is performed with our new software SproutCounter. As input, SproutCounter takes six images from different layers for each well. These images are then scanned for regions that contain isolated beads. Subsequently, spheres are placed around the extracted beads, and intensity values from the spheres are transformed into vectors, which are then subject to several smoothing steps. Finally, the numbers of peaks in the vectors are determined as estimates for the number of sprouts that emerge from the cells on the beads.

Bead identification. To allow for individual analysis of the beads, they have to be extracted from the images. Several imaging steps are performed to reach this goal. First, the layer with the highest contrast value is chosen to simplify bead detection (Fig. S2*B*). For this purpose, for each layer $l \in L$ a contrast value C_l is determined (Eq. **1**).

$$C_l = \frac{1}{|P_l|} \sum_{p \in \mathbf{P}_l} \sum_{q \in \mathbf{Q}_p} \mathrm{Int}(q). \qquad \textbf{[S1]}$$

In Eq. **1**, $\mathrm{Int}(q)$ stands for the intensity value of pixel q, where Q_p is the set of all pixels adjacent to $p \in P_l$. P_l is the set of pixels in layer l with an intensity larger t, where t is a threshold that is linearly dependent on the background intensity bgi of the images (Eq. **2**).

$$t = \mathrm{bgi} * a + b. \qquad \textbf{[S2]}$$

The parameters a and b depend on the average difference between background intensity and bead intensity (default values: $a = 1.5$, $b = 0$); bgi is defined as the average pixel intensity of all layers. To reduce the influence of outliers, pixels are sorted according to intensity prior to bgi calculation and only the middle $g\%$ (default value: $g = 60$) of the pixels is taken into account.

The image with the highest contrast value is then transformed into a binary matrix, where each entry represents a pixel p (Fig. S2*C*). If the intensity $\mathrm{Int}(p)$ is larger t, the entry is set to *true*, otherwise it is set to *false*. The matrix is further processed by setting all entries to *false* that have more than two adjacent *false-set* entries. The latter step, which we call "shrinking", is repeated for a user-defined number of times (default value: 5) and leads to clusters of *true-set* pixels that represent core regions of the beads (Fig. S2*D*). Clusters are identified by a breadth-first-search and coordinates of the image sections around the clusters are extracted. The size of the extracted image section depends on an extension factor m (default value: $m = 0.5$), as well as the width w and height h of the cluster under consideration. A rectangle is placed around the cluster so that the edges of the frame cover the outermost coordinates of the cluster. Then, width and height of the rectangle are elongated at each corner by mw and mh, respectively (Fig. S2*E*).

To avoid processing of incorrectly extracted or not fully extractable beads such as beads that are located at the edge of the images, different filters are applied. Also, particularly large, small, and not approximately quadratic clusters are discarded.

Sprout counting. For each of the extracted image sections, contrast values C_l are recalculated. The layer with the highest contrast value C_{ref} serves as reference image for the respective section and is used for sphere placement. For this purpose, the local intensity threshold tloc has to be determined on the basis of the local background intensity $\mathrm{bgi}_{\mathrm{loc}}$ (Eq. **3**).

$$t_{\mathrm{loc}} = \mathrm{bgi}_{\mathrm{loc}} * a_{\mathrm{loc}} + b_{\mathrm{loc}}. \qquad \textbf{[S3]}$$

Since the major part of the extracted image sections are covered by beads, $\mathrm{bgi}_{\mathrm{loc}}$ is determined differently from bgi. $\mathrm{bgi}_{\mathrm{loc}}$ is defined as the first quartile of the lower half of the increasingly sorted pixel intensities of the image section (the first octile). The geometric center of a bead is calculated by averaging over the position of all pixels within the inner 60% of the image section that have an intensity larger t_{loc}.

To determine the radius of the bead under consideration, 180 individual calculations are performed in 2° rotation-steps, each measuring the distance from the center to the edge of the bead. Along 180 uniformly distributed lines that emerge from the center and end at the image section border, pixel intensities are measured and stored in 180 vectors $v \in V$. The first entry in a vector v relates to the intensity of the center, the last entry to the intensity of the pixel at the edge of the image section. For each vector, the distance d_v from the bead's center to its edge is defined as the smallest index of v with intensity smaller t_{loc}, where both preceding and both following values of v are smaller than t_{loc} as well (Eq. **4**).

$$d_v = \arg\min_k \{v[k-2] < t, v[k-1] < t, \ldots, v[k+2] < t\}. \qquad \textbf{[S4]}$$

The average distance $\bar{d}$ of all distances d_v is taken as radius for the bead under consideration. If the standard deviation of distance values d_v is larger than a user-defined threshold (default value: $0.2 * \bar{d}$), the bead is regarded invalid and excluded from further analysis.

For the actual quantification of sprouting, a sphere is placed around the body of the bead (Fig. S3*A*). The sphere's radius is equal to the radius of the bead plus an additional user defined value r (default value: $r = 7$). All intensity values of layer l that lie on this sphere are stored in a vector x_l (Fig. S3*B*). Sprouts emerging from the cells on the beads that cross the sphere are observable as peaks in the intensity vector. For peak identification several smoothing steps are performed on x_l. First, the local background intensity is subtracted from the intensity values in x_l. For each index i of a vector x_l, values of the neighboring indices $n \in N_i^1$ are determined, averaged, and subtracted from $x_l[i]$ (Eq. **3**). Since the intensity vector represents a sphere, the last element of the vector is the immediate neighbor of the first element and vice versa. The size of the neighborhood is user-determined (default value: $|N_i^1| = 50$).

$$y_l[i] = x_l[i] - \sum_{n \in \mathbf{N}_i^1} x_l[n]. \qquad \textbf{[S5]}$$

During background subtraction, y-values of indices i that are located in close proximity to high intensity peaks become relatively more negative than it is observable in the raw data. This is due to the fact that high intensity values of the neighboring peak indices elevate the average value of the neighborhood. Importantly, since only maxima of the intensity vectors are regarded in the subsequent data analysis these artificial intensity minima do not have a substantial effect on sprout quantification.

After this first preprocessing step, the obtained vector y is smoothed by a sliding window approach, where each entry i gets assigned the average value of all neighboring indices $n \in N_i^2$ in the vector. The size of the neighborhood is user-determined (default value: $|N_i^2| = 15$).

$$z_l[i] = \frac{1}{\mathbf{N_i^2}} \sum_{n \in \mathbf{N}_i^2} y_l[n]. \quad \textbf{[S6]}$$

This step is repeated until smooth vectors are obtained (Fig. S3*B*). Each maximum larger zero represents one sprout that emerges from the bead.

In order to detect sprouts that are not visible in the image layer with the highest contrast value, all layers $l \in L$ that have a contrast value of at least $C_{\text{ref}}/2$ are evaluated as well. The positioning of the sphere is equal in all layers. The intensity vector and smoothing steps are calculated separately. To avoid multiple counting of sprouts that are present in different layers, vector values of all layers are added for each entry j and stored in vector f (Eq. **7**). Finally, all maxima m of the vector f with $f[m] > 0$ are counted as sprouts (Fig. S3*C*).

$$f[i] = \sum_{l \in L} z_l[i]. \quad \textbf{[S7]}$$

Several parameters can be changed by the user to adapt the software to the images that are created by an assay, and the choice of these parameters can have an impact on sprout quantification. For instance, if the radius parameter r is set to small values (e.g., $r = 2$), parts of the sphere might intersect with the bead leading to noise in the data. If contrariwise r is set to large values (e.g., $r = 12$), short sprouts emerging from the cells on the beads might not be detected. To check whether sprout quantification is sensitive to changes in the parameters, we exemplarily performed a systematic analysis of the radius parameter r. We analyzed the method′s ability to discriminate between inducing (S1P+VEGF-A+bFGF) and inhibiting sprouting conditions (S1P+VEGF-A +bFGF plus sunitinib) with various radii r. For both technical replicates the signal-to-noise ratio improved with increasing values of r reaching stable discrimination for $r > 5$ (Fig. S3*D*). To reduce the risk that spheres intersect with sprouts emerging from cells on beads in close proximity, an acceptably small stable value was chosen ($r = 7$). Parameters affecting the smoothing of the intensity vectors can also have impact on sprout quantification. If the neighborhood size is set to large values (e.g., $N_i^2 = 40$) only sprouts with high observable intensity are detected, while for small values (e.g., $N_i^2 = 5$) also subtle intensity changes in the vector are counted as sprout. The here employed empirically determined neighborhood size of $N_i^2 = 15$ serves as a trade-off between both extrema and showed stable performance in terms of signal to noise ratio for the 54 plates of both runs (Fig. S5 *A* and *B*).

In vivo Matrigel plug assay. Eight-week-old female FvB mice (Charles River) were anesthetized with a ketamin (50 mg/kg body weight, Vetoquinol) medetomidine (0.15 mg/kg body weight, Orion Corp.) mixture and shaved for Matrigel injection. 400 μl of 9.5 mg/ml growth factor reduced Matrigel (BD Biosciences) supplemented with either 500 ng/ml vascular endothelial growth factor (VEGF)-A, 500 ng/ml basic fibroblast growth factor (bFGF) and 2 μM sphingosine-1-phosphate (S1P), or with phosphate-buffered saline (PBS) as vehicle control were injected subcutaneously into both abdominal flanks, resulting in two Matrigel plugs per animal. Seven mice per group were treated every 24 h by intraperitoneal injection with either 5% DMSO in PBS (controls) or simvastatin (2 mg/kg body weight) or U0126 (15 mg/kg body weight) starting from the day of Matrigel implantation. After 21 d, mice were killed by anesthetics overdose, shaved, and the Matrigel plugs including the overlying skin generously removed, immediately embedded in optimal cutting temperature compound (Sakura Finetek) and snap frozen. Cryosections (7 μm thickness) were fixed in acetone/methanol. Slides were blocked and double-immunostained with primary rabbit anti-mouse LYVE-1 antibody (Angiobio) and rat anti-mouse CD31 antibody (BD Biosciences) in antibody diluent (Zytomed) for 1 h at room temperature. Primary antibodies were detected with secondary donkey anti-rabbit Alexa 488 conjugated and donkey anti-rat Alexa 594 conjugated antibody (Invitrogen) as described (1). Samples were mounted with Mowiol (Polysciences) and dried before being imaged on an epifluorescence Axioskop 2 mot plus microscope equipped with a Plan-APOCHROMAT 10x/0.45 objective, and an AxioCam MRc camera under 488 nm and 594 nm filters with the Axio-Vision software Version 4.7.1 (all Carl Zeiss). Five frames per Matrigel plug were analyzed for both plugs per animal. Lymphatic vessels were identified as CD31/LYVE-1 double positive structures with a characteristic, elongated morphology to exclude LYVE-1+/CD31- macrophages and unspecifically stained stratum corneum and hair follicles. Lymphatic vessel number and area were quantitated with ImageJ (National Institutes of Health) and normalized to mm epidermal basement membrane (BM) at the interface of dermis and epidermis visible without additional staining (Fig. 5*B*) or to % dermis (Fig. 5*D*). Mouse studies were performed according to Swiss law and approved by the Veterinäramt of the canton Zurich under permission number 149/2008.

In vivo cornea assays. Eight-week-old male BALB/c mice (Taconic Farms) were treated according to Association for Research in Vision and Ophthalmology Statement for the Use of Animals in Ophthalmic and Vision Research. All protocols were approved by the Animal Care and Use Committee, University of California, Berkeley. Mice were anesthetized using a mixture of ketamine, xylazine, and acepromazine (50, 10 mg, and 1 mg/kg body weight, respectively) for each surgical procedure. Our standard suture placement model was used to induce corneal inflammatory lymphangiogenesis, as described previously (2–4). Briefly, three 11-0 nylon sutures (AROSurgical) were placed into the stroma of central corneas without penetrating into the anterior chamber. Mice were randomized to receive systemic administrations of simvastatin (2 mg/kg of body weight) or control vehicle twice a week for two weeks. The experiments were repeated twice with a total of eight mice in each group of study. Staining and analysis was performed as described previously (3, 4). Briefly, whole-mount fresh corneas were excised at 14 d after the suture placement and fixed in acetone for immunofluorescent staining. Nonspecific staining was blocked with donkey serum (Jackson ImmunoResearch Laboratories Inc.). The samples were stained with a purified rabbit anti-mouse LYVE-1 antibody (Abcam), which was visualized by a Cy-3 conjugated donkey anti-rabbit secondary antibody (Jackson ImmunoResearch Laboratories Inc.). Stained samples were examined and photographed with an epifluorescence microscope (AxioImager M1, Carl Zeiss). Lymphatic vessels were graded and analyzed using ImageJ. The lymphatic area was normalized to the total corneal area to obtain a percentage coverage score for each sample.

Cancer cell invasion assay. The LEC bead sprouting assay was adapted for metastatic MDA-MB-231 mammary carcinoma cells with the following changes: Beads were coated at a bead:cell ratio of 1:80 and cell invasion was induced with 40 ng/ml VEGF-A and bFGF.

1. Huggenberger R, et al. (2011) An important role of lymphatic vessel activation in limiting acute inflammation. *Blood* 117:4667–4678.
2. Truong T, Altiok E, Yuen D, Ecoiffier T, Chen L (2011) Novel characterization of lymphatic valve formation during corneal inflammation. *PLoS ONE* 6:e21918.
3. Yuen D, Pytowski B, Chen L (2011) Combined blockade of VEGFR-2 and VEGFR-3 inhibits inflammatory lymphangiogenesis in early and middle stages. *Invest Ophthalmol Vis Sci* 52:2593–2597.
4. Grimaldo S, Yuen D, Ecoiffier T, Chen L (2011) Very late antigen-1 mediates corneal lymphangiogenesis. *Invest Ophthalmol Vis Sci* 52:4808–4812.

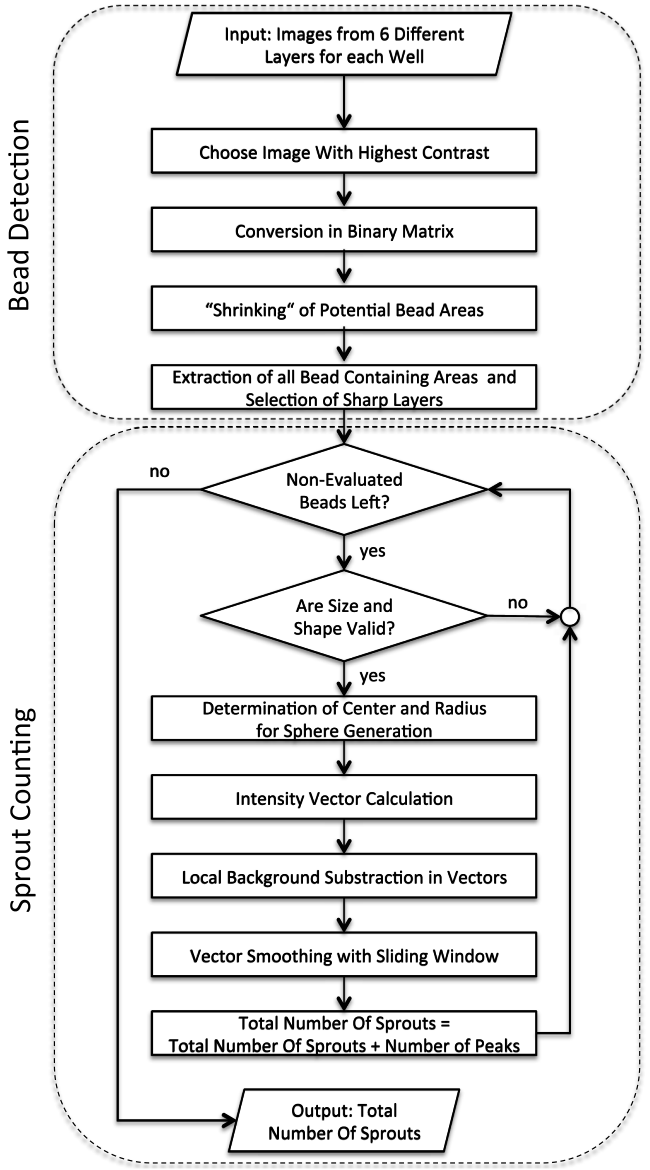

Fig. S1. Workflow of the SproutCounter algorithm. First, beads are extracted from the images. Subsequently, sprout counting is performed for each bead to result in a sprout # per bead.

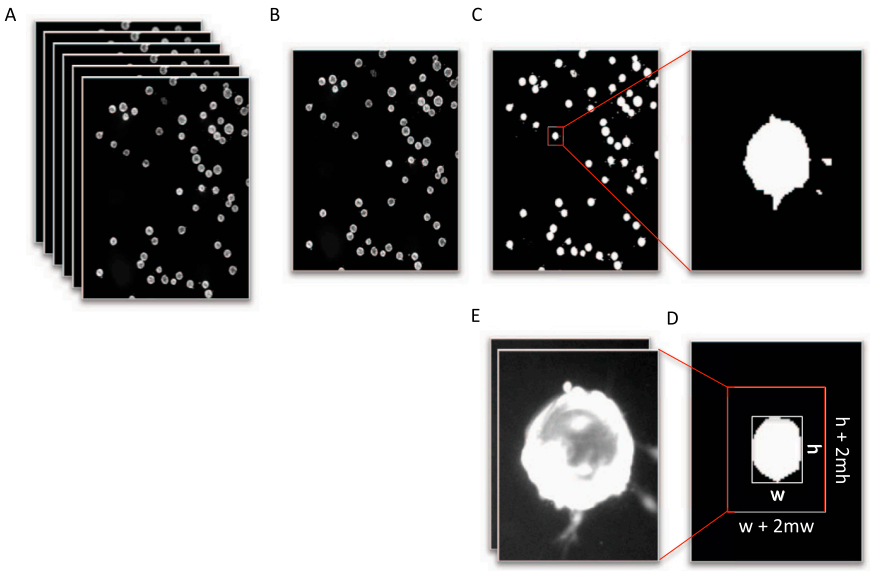

Fig. S2. Bead extraction procedure. (*A*) Input consists of images from six layers with an increment of 30 μm. (*B*) Selection of image with highest contrast. (*C*) Binarization of the reference image. (*D*) "Shrinking" of potential bead clusters and determination of bead core region. (*E*) Extraction of image section that contains bead. Layers that are out of focus are not considered for sprout counting. For more detail refer to *SI Materials and Methods*.

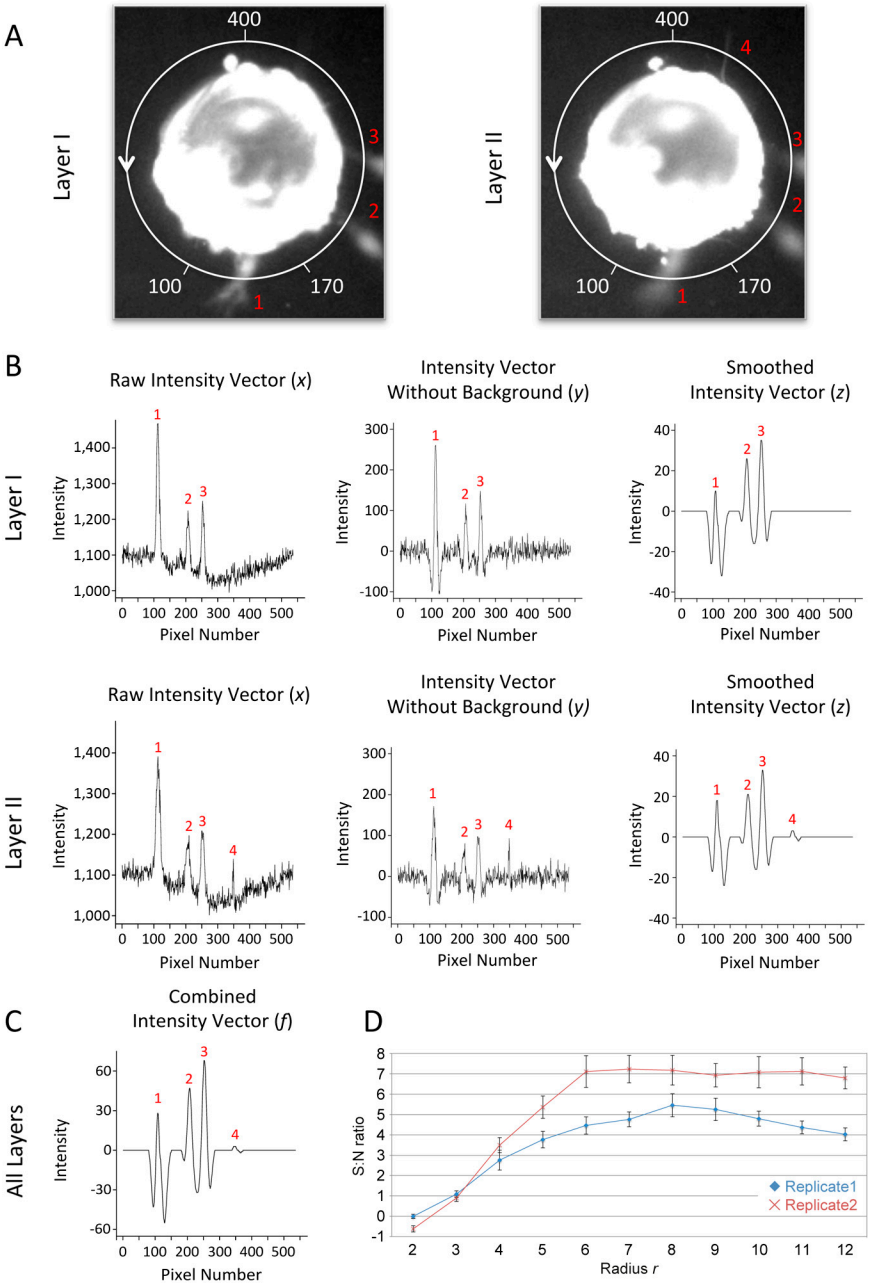

Fig. S3. Counting of the number of sprouts that emerge from a bead. (*A*) A sphere is placed around the body of the bead in each layer. (*B*) Intensities along the spheres are transformed into vectors. Subsequently, vectors are smoothed by a sliding window approach. (*C*) Vector values of all layers are summed up to build the final vector *f*. The number of peaks with an intensity >0 in *f* serves as estimate for the number of sprouts emerging from the cells on the bead. (*D*) Influence of radius *r* on the "signal-to-noise ratio" (S:N ratio). Screening was performed with a default value of $r = 7$. For more detail refer to *SI Materials and Methods*.

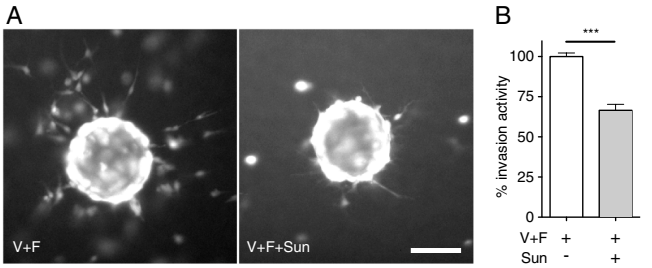

Fig. S4. The bead sprouting assay and SproutCounter software can be adapted to a cancer cell invasion assay. (*A*) Epifluorescence micrographs of cell tracker green labeled MDA-MB-231 cells on beads 24 h after induction with V+F demonstrate pronounced cell invasion of surrounding collagen type I hydrogel for

control that was reduced by addition of sunitinib. Scale bar represents 100 μm. (*B*) Automated quantification of gel-invading cells by SproutCounter software gave a clear separation between control and sunitinib treated cells. *** $p < 0.001$ in unpaired Student t-tests ($n = 10$). V + F = VEGF-A(40 ng/ml)+ bFGF(40 ng/ml); Sun = Sunitinib (5 μM). Bars show mean ± SEM.

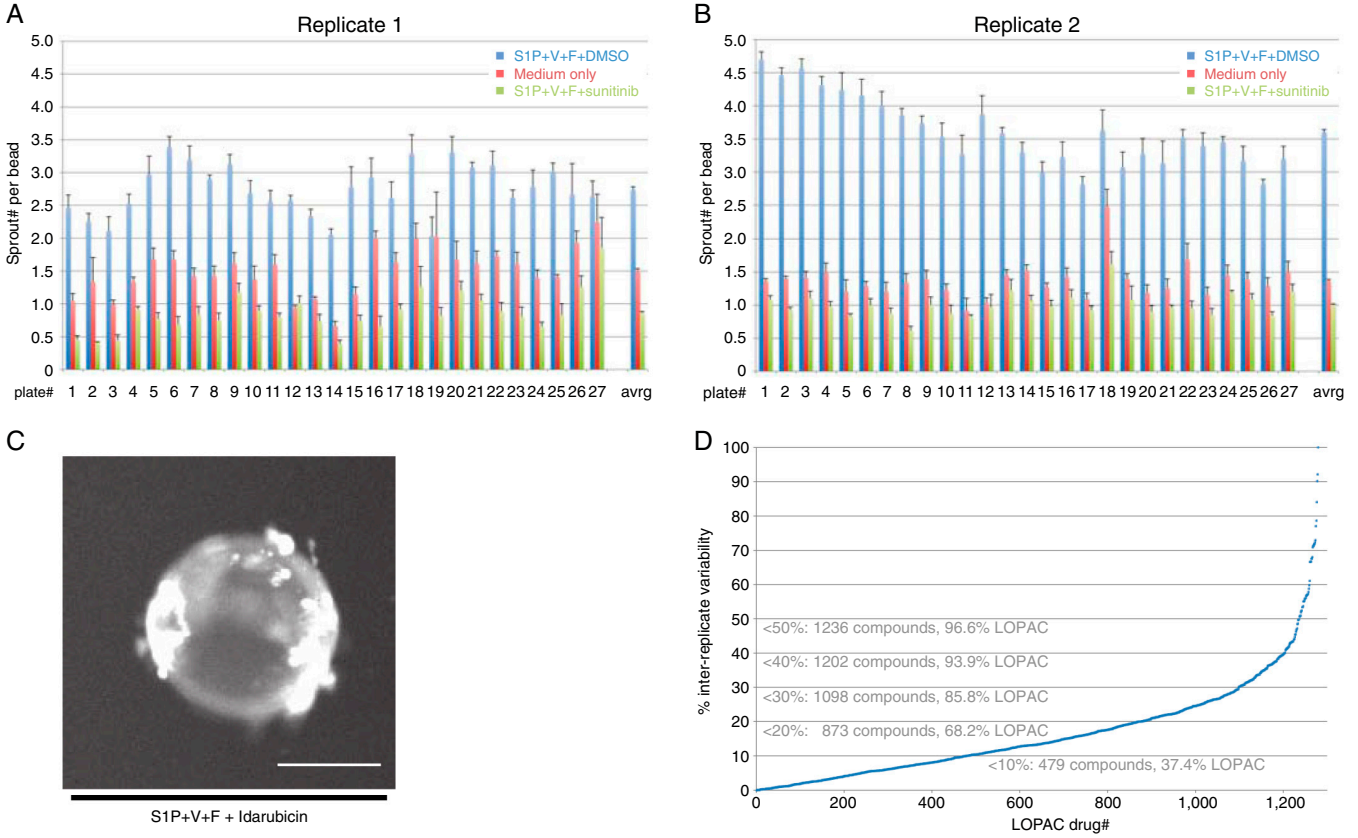

Fig. S5. Library of Pharmacologically Active Compounds (LOPAC)[1280] screen quality control. (*A* and *B*) Control distribution. Negative (blue bars), baseline activity (red bars), and positive (green bars) control means (±SEM) for each individual plate (1–27) and over all plates (avrg) are plotted as sprout number per bead for both screening replicates demonstrating a clear control separation. (*C*) Cytotoxicity control. A representative frame of idarubicin treated beads from the screen demonstrates loss of physiological morphology and EC bead coverage. (*D*) Inter-replicate variability. Distribution of the 1,280 LOPAC compounds by their % variability between replicate 1 and 2 are plotted (blue dots) with percentiles (gray text) demonstrating a low inter-replicate variability for a majority of compounds. Drugs are sorted from left to right with increasing difference between replicate 1 and replicate 2. S1P + V + F = S1P(2 μM)+ VEGF-A(40 ng/ml) + bFGF(40 ng/ml); avrg = control mean from all 27 plates. Scale bar represents 100 μm.

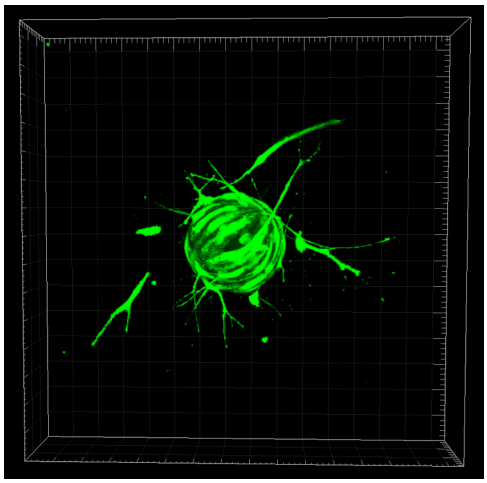

Movie S1. Confocal 3D reconstruction of sprouting LEC-covered bead. Cell tracker green labeled LECs on beads were encapsulated in collagen gels in Labtek chamber slides and treated with S1P(2 μM) + VEGF-A(40 ng/ml) + bFGF(40 ng/ml) for 24 h. High resolution z-stacks of sprouting beads were acquired by confocal microscopy and 3D reconstructions produced by Imaris software. Major ticks represent 30 μm.

Movie S1 (MOV)